Extinction with 2MASS: star counts and reddening toward the North America and the Pelican Nebulae

L. Cambrésy

Infrared Processing and Analysis Center, Jet Propulsion Laboratory, California Institute of Technology, M/S 100-22, Pasadena, CA 91125

laurent@ipac.caltech.edu

C. A. Beichman

Jet Propulsion Laboratory, California Institute of Technology, M/S 180-703, Pasadena, CA 91109

chas@pop.jpl.nasa.gov

T.H. Jarrett and R. M. Cutri

Infrared Processing and Analysis Center, California Institute of Technology, M/S 100-22, Pasadena, CA 91125

jarrett@ipac.caltech.edu,roc@ipac.caltech.edu

ABSTRACT

We propose a general method for mapping the extinction in dense molecular clouds using 2MASS near-infrared data. The technique is based on the simultaneous utilization of star counts and colors. These two techniques provide independent estimations of the extinction and each method reacts differently to foreground star contamination and to star clustering. We take advantage of both methods to build a large scale extinction map ($2.5^\circ \times 2.5^\circ$) of the North America-Pelican nebulae complex. With K_s star counts and $H - K_s$ color analysis the visual extinction is mapped up to 35 mag. Regions with visual extinction greater than 20 mag account for less than 3% of the total mass of the cloud. Color is generally a better estimator for the extinction than star counts. Nine star clusters are identified in the area, seven of which were previously unknown.

Subject headings: ISM: clouds — dust, extinction — ISM: individual (North America Nebula, Pelican Nebula) — infrared: ISM — stars: formation

1. Introduction

The knowledge of the extinction in molecular clouds is essential for a wide range of purposes. The extinction traces the dust distribution and thus provides an estimate of the column density of hydrogen that can be compared to the far-infrared or submillimeter emission from dust and to molecular emission lines. Fundamental properties are derived from these comparisons. Stepnik et al. (2001) have found evidence of dust evolution in a translucent cloud in Taurus using extinction from J-2MASS star counts and submillimeter data from the balloon-borne experiment PRONAOS. Kramer et al. (1999) have compared the $C^{17}O$ line with extinction derived from $H-K$ color and have found a depletion of CO for $A_V > 10$ which indicates the interaction between dust an gas in high density regions. The dust distribution also gives information about the fragmentation processes which may be responsible for the shape of the initial mass function (Padoan et al. 1997b) through turbulent motions in the interstellar medium (Padoan et al. 1997a). All these results were obtained with near-infrared data which are better adapted than optical wavelengths for extinction studies. 2MASS provides accurate ($\sim 3\%$) J, H and K_s photometry for the whole sky. The K_s band is about 10 times less absorbed than the V band making possible to analyze the dust distribution for visual extinctions as large as 40 mag. Since the dust both absorbs and reddens the starlight, the analysis of the star density and star color variations give two independent estimates of the extinction. In this paper, we take advantage of these two techniques to measure the extinction and understand better the limitations of each method.

The first section of this paper describes the methods for mapping the dust distribution based on K_s star counts and $H-K_s$ reddening. The comparison of the two maps leads to the identification of foreground stars and stellar clusters. In a second section, we apply our technique to the North America-Pelican complex which is located in the galactic plane at an intermediate distance (~ 580 pc). By analyzing the statistical and systematic uncertainties in the star count and in the color extinction maps we merge these two maps into a more reliable representation of the cloud. We also propose the identification of new stellar clusters in this complex field. In the appendix, we discuss the comparison between 2MASS data and a synthetic model for stellar populations.

2. Extinction mapping

2.1. Star counts

Variation of the star density across the sky was the first observable indication of extinction, i.e. of presence of dust in the Galaxy. Star counts are therefore the oldest method

of mapping the interstellar cloud extinction (Wolf 1923). The method consists of counting stars in magnitude intervals in each cell of a regular grid in an obscured field and comparing this number with the counts in a reference field, supposedly free of absorption. To improve the spatial resolution, Bok (1956) made counts up to the limiting magnitude rather than in magnitude intervals. Manual techniques were used on Schmidt plates for many decades (Dickman 1978; Cernicharo & Bachiller 1984; Mattila 1986; Gregorio Hetem et al. 1988; Andreazza & Vilas-Boas 1996). More recently Cambrésy et al. (1997) proposed a variant of the classical method by replacing the regular grid by an adaptive grid. They used infrared data from the DENIS survey (Epchtein 1997) and an automatic counting technique that is possible with digital data. The adaptive grid optimizes the angular resolution with respect to the local star density. This is useful when there are significant fluctuations of density due to large extinction gradients or the presence of star clusters.

In its simplest form, star count method assumes that all stars are behind the cloud and that the stellar population is homogeneous for the whole field. Moreover, the star density is supposed to be uniform within a cell. Cloud structures on angular scales smaller than the resolution of unit cell can lead to underestimates of the extinction (Rossano 1980; Thoraval et al. 1997). From star counts in the K_s band, the visual (V) extinction is derived from star density (D) as follows:

$$A_{K_s} = \frac{1}{a}\log\frac{D_{\rm ref}}{D} = \mathcal{Z} + \frac{1}{a}\log\frac{1}{D} \quad (1)$$

$$A_V = \frac{A_V}{A_{K_s}} \times A_{K_s} \quad (2)$$

where a is the slope of the K_s luminosity function and $D_{\rm ref}$ the density in a reference field. Since the reference density depends on the position (mainly on the galactic latitude), we use a *zero point function*, $\mathcal{Z}$, which can be approximated by a constant value only for small areas (typically less than 1 deg^2). For larger areas, $\mathcal{Z}$ is estimated using a fit of the uncalibrated A_V versus galactic position for unobscured regions close to the cloud.

2.2. Reddening

Dust that obscures also reddens starlight. Measuring the reddening of stars behind a cloud gives the extinction along the line of sight. The spatial resolution of the derived extinction is very high and corresponds to the apparent size of the stellar disk, but the measurements are strongly undersampled. The reddening is the difference between the observed star color and the intrinsic color corresponding to the star spectral type. Frerking et al. (1982) used $J-K$ color to map the extinction toward fields in ρ Ophiuchus and Taurus.

Jones et al. (1984) used the same color to map the extinction in a Bok globule toward the Southern Coalsack. Until recently, the necessity of knowing the spectral type precluded a wide use of this method. However, with the advent of large digital surveys like 2MASS, statistical studies become possible where the knowledge of the spectral type is replaced by the measure of the mean color in an unobscured field. Using 2MASS prototype data, Beichman & Jarrett (1994) derived the extinction toward the Taurus cloud by comparing $J-H$ and $H-K_s$ colors to a galactic model of stellar populations. Lada et al. (1994) proposed a method based on the $H-K$ averaged color in a regular grid to map highly extinguished clouds with visual extinction up to 30-40 mag (Alves et al. 1998; Lada et al. 1999). Using DENIS data Schultheis et al. (1999) mapped the extinction toward the galactic center with a sophisticated method based on the isochrone position in a $J-K_s/K_s$ color-magnitude diagram.

As for star counts, a homogeneous population is assumed for the reddening analysis. Stars must lie behind the cloud and the reddening is supposed to be uniform within a cell. For example, the study of Schultheis et al. (1999) in the direction of the galactic center was restricted to RGB/AGB stars; they selected a specific stellar population at a large distance (behind the galactic center).

We have chosen to use the $H-K_s$ color because it presents a small intrinsic dispersion over typical stellar spectral types. Typically, we have $0 < H-K_s < 0.37$ (Bessell & Brett 1988) and a single peak in the color distribution. The $J-K_s$ color has separate peaks for dwarf and giant stars which makes it difficult to convert a mean color to an extinction.

We propose here an adaptive variant of the Lada's method. The size of our cells change with the local stellar density and is varied to contain always the same number of stars detected in both H and K_s 2MASS bands. The motivation for using adaptive cells is the same as that mentioned for star counts: to optimize the angular resolution for large variations of extinction and increase the resolution around stellar clusters. Visual extinction is derived as follows:

$$E_{H-K_s} = (H-K_s)_{\rm obs} - (H-K_s)_{\rm int} \quad (3)$$

$$A_V = \left(\frac{A_H}{A_V} - \frac{A_{K_s}}{A_V}\right)^{-1} \times E_{H-K_s} \quad (4)$$

where $(H-K_s)_{\rm obs}$ is the observed median color in the cell and $(H-K_s)_{\rm int}$ is the observed median color in the reference field and represents the intrinsic median color for unreddened stars. This differs from the Lada's method in which mean color is used rather than median color. Our choice is driven by the foreground star correction that is discussed in section 2.3.2. Color is less sensitive to galactic latitude than star counts and a constant characteristic value (e.g. zero point of extinction) is correct for several square degrees. On larger scales,

the dependence with the galactic latitude (and longitude) must be taken into account with a zero point which is a function of direction.

2.3. Simultaneous use of the two methods

2.3.1. Calibration

To use both star counts and reddening to study a cloud it is necessary to ensure that the calibrations are consistent. First, the spatial resolution must be identical, i.e. same cells must be used. Practically, the cell size is adapted to contain a number of stars, N, detected in both H and K_s. The K_s star density is measured in the cell (number of K_s stars divided by the cell surface area) and the $H - K_s$ color of the N stars is represented by their median value.

Star counts and colors are converted into extinction using equations (1)-(4). Since the zero point of the color-based extinction map is more reliable than that of the star counts-based map due to a weaker dependence on galactic latitude, the star counts map is adjusted to the zero point of color map. The larger the area free from absorption used, the better is the adjustment.
For a small field (~ 1 deg^2), the difference between the maps is simply an offset. For a large cloud ($\lesssim 100$ deg^2), a linear fit of the difference between the two maps versus the galactic latitude is required. For still larger sizes, variation with the galactic longitude may also occur and the galactic latitude fit may no longer be linear.

2.3.2. Expected differences

Once the extinction maps are constructed with a consistent calibration, significant differences are still expected because each method has its own behavior when the *a priori* assumptions are not valid.

Effect of foreground stars

Star counts. Foreground stars are not affected by the cloud extinction and their number density, N^f, does not vary; whereas the background star density, N^b, is affected by the extinction as described in equation (1): $N^b = N_0^b \times 10^{-a\,A_{K_s}^{\rm real}}$, where a is the K_s luminosity function slope and the 0 subscript refers to zero-extinction stellar density. The observed

extinction can be written:

$$A_{K_s}^{\rm obs} = \frac{1}{a}\log\frac{N_0^b+N_0^f}{N^b+N_0^f} \quad (5)$$

$$= \frac{1}{a}\log\frac{N_0^b+N_0^f}{N_0^b\times 10^{-a\,A_{K_s}^{\rm real}}+N_0^f} \quad (6)$$

Let X be the fraction of background stars, $X = N_0^b/(N_0^b+N_0^f)$, we have:

$$A_{K_s}^{\rm obs} = -\frac{1}{a}\log\left(X\,10^{-a\,A_{K_s}^{\rm real}}+(1-X)\right) \quad (7)$$

Foreground stars reduce the density contrast between low and high extinction regions. For a given X, the measured extinction cannot exceed $-1/a\times\log(1-X)$, even for an infinite real extinction. For example, with $X = 0.9$ the observed visual extinction cannot exceed 26 mag from K_s star counts (10.5 mag from J star counts and 3 mag from V star counts).

Reddening. Since the color in a cell is represented by the median color of the stars it contains, the contamination by foreground stars makes the derived extinction drop to zero when more than half of the stars are in front of the cloud (i.e. when the median color corresponds to the foreground star color). This happens at the wavelength λ for $A_\lambda = -1/a\log[(1-X)/X]$. In the H band, which is the most affected by extinction, the turn over occurs at $A_V \approx 16$ mag for $X = 0.9$.

Foreground star suppression. In Figure 1, the *observed* extinction is plotted versus the *true* extinction for a fraction of background stars X. The star count plots are obtained using equation (7). The color excess plot is obtained assuming a color distribution characterized by $H-K_s = 0.17\pm0.1$ mag that corresponds to the value obtained with the stellar population model described in the appendix, for a direction close to the galactic plane ($l = 85°$, $b = -1°$). As expected, K_s star counts give better results for high extinction than J star counts because of the relative sensitivity to the extinction ($A_J/A_{K_s} \approx 2.5$). The color excess technique is definitely more robust to foreground star contamination than star counts until the number of background stars drops to equal the number of foreground stars.

Consequently, for high extinction, $A_V \sim 20$ mag and $X = 0.9$, K_s star counts give a much higher extinction (≈ 15 mag) than does $H-K_s$ reddening (almost 0 mag). The star count extinction map would show an extinction peak where the reddening map would show a hole in the cloud. Using the two maps allows one to show that the extinction is so high that there are more foreground stars than background stars in a particular direction.

The foreground star density can be estimated from these directions using the $J - K_s$ color, which is the most sensitive to extinction. Once the foreground star density is known, we can remove these objects for each direction assuming that they are the bluer (i.e. lower $J - K_s$) population. This hypothesis is verified only for high extinction regions, where the reddening is larger than the total uncertainties in the two maps. For low extinction, removing the bluer stars introduces a bias that will be discussed later (§ 3.3). When foreground stars are removed from the catalog, the star counts and the reddening analysis must be iterated to build reliable extinction maps for which the foreground star contamination is corrected.

Young stellar clusters

Molecular clouds are star forming regions and young embedded star clusters are to be expected in such areas. A cluster produces an artifact in the star count extinction map: the excess density is interpreted as a hole in a cloud. On the other hand, such clusters generally contain stars with an intrinsic infrared excess due to an envelope or an accretion disk (especially for low-mass stars) which leads to an extinction peak in a $H - K_s$ color extinction map.

This is the opposite situation that was encountered for the contamination by foreground stars: the extinction appears larger in the color map than in the star count map. Directions for which the star density is significantly too large compared to the color suggest the presence of star clusters. A similar approach is developed in Carpenter (2000) who identifies young clusters by comparing 2MASS K_s star counts to stellar densities predicted by a model toward Perseus, Orion and Monoceros R2 molecular clouds and using CO line to correct for the extinction.

3. Application to the North America-Pelican nebulae

3.1. 2MASS data

The 2MASS survey provides near–infrared photometry in the J, H and K_s filters. At the time of this paper data covering, 48% of the sky has been released through the 2$^{\rm nd}$ Incremental Data Release (Cutri et al. 2000) and 100% of the sky has been observed. Since data analyzed here are not in the 2$^{\rm nd}$ release, we have extracted the catalog directly from the point source working database which contains sources extracted in each Tile (a 2MASS unit of $8.5' \times 6^\circ$ obtained by the co-addition of 274 images). As distinguished from the 2$^{\rm nd}$ release Point Source Catalogue, the working database contains multiple entries for the same star in

Tile overlap regions, low signal-to-noise sources, and artifacts flagged during the processing. We have extracted from the point source working database sources that satisfy the following criteria which are similar to the criteria used to generate the point source catalogue:

1. photometric uncertainty $\sigma < 0.25$
2. signal-to-noise greater than 7 in at least one band
3. no filter glint flag (ghost sources that occur at specific geometric locations relative to bright stars)
4. no diffraction spike flag
5. persistence probability due an echo of a previously observed bright star < 0.5 in the 3 bands simultaneously

In this filtering, we kept sources bright enough to be accepted as a real source but weakly contaminated by a diffraction spike, and sources with high PSF fitting χ^2 (generally due to confusion between two stars). We give preference to completeness rather than reliability because our analysis is statistical and involves star counts.

Redundant source entries in the Tile overlaps were removed by filtering out sources within $3''$ of bright stars (brighter than 8.5 mag in one band) and within $1.5''$ of fainter stars. The final catalog contains about 1.1×10^6 objects.

Based on an estimate of completeness from the magnitude distribution, Figure 2, we kept only stars brighter than $K_s < 15.0$ mag for the star count analysis and stars brighter than $H < 15.5$ mag and $K_s < 15.0$ mag for the color analysis. Analysis of repeated observations of calibration fields observed ~ 100 times indicates that the integral 2MASS completeness for these magnitudes is $\sim 99\%$ (Cutri et al. 2000). The density and color distribution of the selected stars does not show any residual persistence of the 2MASS observing Tiles. This validates the *catalog extraction* from the database and the adopted limiting magnitudes. An incorrect treatment of multiple entries in the working database would have led to the detection of the Tile overlaps in the density map while an overestimation of the limiting magnitudes would have introduced a star density level difference between Tiles, especially for those observed at different dates, under different airmass and/or atmospheric conditions. To derive extinction from K_s star counts using equation (1) the slope of the luminosity function, a, is needed. Its estimate from Figure 2 is $a = 0.34$.

3.2. Cloud properties

The cloud studied in this paper lies between two HII regions, the North America nebula (NGC 7000) and the Pelican nebula (IC 5070). This complex is also named W80 (Westerhout 1958) and the dark cloud itself is known as L935 (Lynds 1962). In the following, we use NAN to refer to the whole complex. Visual extinction has been deduced from Hα surface brightness by Goudis & White (1979) who found a *maximum* visual extinction of about 8 mag. Bally & Scoville (1980) performed ^{12}CO observations of the cloud and proposed an evolutionary scenario for the molecular cloud. They concluded that the cloud is highly fragmented and contains an expanding molecular shell. Wendker et al. (1983) proposed a model to described the whole complex based on radio continuum observations. They gave a distance estimate of 500 pc. This distance has been confirmed by Straižys et al. (1993) who obtained $d = 580$ pc using photoelectric photometry of 564 stars in the direction of the complex. The total mass of the cloud has been estimated from molecular observations (^{12}CO, ^{13}CO and H_2CO) to be 5×10^4 $M_\odot$ (Feldt & Wendker 1993).

Herbig (1958) discovered 68 stars having the Hα line toward the complex, suggesting the existence of a population of Be (intermediate mass) and T Tauri (low mass) stars. Della Prugna et al. (1984) reobserved these sources to provide more accurate astrometry. Welin (1973) and Marcy (1980) discovered additional Hα emission stars in the NAN. The total number of previously known young stars in the square area defined in the Figure 3 is 119.

To clearly delimit the dark cloud, we performed the star counts and the color analysis on a large area around the cloud: 5.6° diameter centered on $\alpha_{\rm J2000} = 10^{\rm h}56^{\rm m}00^{\rm s}$, $\delta_{\rm J2000} = 44°43^{\rm m}43^{\rm s}$. However, the extinction study is restricted to a 2.5°×2.5° area centered on $\alpha_{\rm J2000} = 20^{\rm h}54^{\rm m}05^{\rm s}$, $\delta_{\rm J2000} = 44°13^{\rm m}57^{\rm s}$ ($l = 84.9$, $b = -0.41$). The optical image and $J - K_s$ map of the large region are presented in Figure 3. $J - K_s$ color is more sensitive to low extinction than $H - K_s$ and shows the general shape of the dark cloud. The reference field to set the zero point of extinction has been chosen in the area of lower $J - K_s$ value. It contains 20,000 stars detected in both H and K_s.

3.3. Results

In the following, we assume the Rieke & Lebofsky (1985) extinction law rather than the most widely used Cardelli et al. (1989) law because the former is in better agreement with the reddening vector slope measured in the 2MASS color-color diagram ($H - K_s/J - H$) obtained for the NAN (Figure 4). We have measured a slope of 1.61 ± 0.32 and Rieke & Lebofsky (1985) and Cardelli et al. (1989) obtained 1.70 and 1.21, respectively. We will

therefore use the following values: $A_J/A_V = 0.282$, $A_H/A_V = 0.175$ and $A_{K_s}/A_V = 0.112$.

3.3.1. Extinction

Reddening method

The extinction map of the NAN is obtained using $H - K_s$ color with the method described in § 2.2. The average color in the reference field provides the absolute calibration of the extinction (zero point). The average color in the reference region is $(\overline{H - K_s})_{\rm int} = 0.16$, with a dispersion (1 σ) of 0.12 mag which corresponds to $A_V = 1.9$ mag. The dispersion represents the sum of the photometric uncertainties, the intrinsic dispersion due to the average over all spectral types and a possible contamination by a residual absorption is the field. This dispersion is consistent with the one obtained using the galactic model presented in the appendix (0.1 mag), suggesting that there is no significant extinction contamination in the reference field. To estimate the systematic error resulting from a possible residual absorption one can use the hydrogen column density. Molecular hydrogen column density can be derived from the CO emission. For this field $W({\rm CO}) = 0.03$ K km s^{-1} (Dame et al. 2001) which corresponds to $N({\rm H_2}) = 5.4 \times 10^{18}$ cm^{-2}. The atomic hydrogen column density is obtained from the 21 cm emission line and is $N({\rm HI}) = 3.7 \times 10^{21}$ cm^{-2} (Leiden/Dwingeloo survey, Burton & Hartmann 1994). This value represents the total hydrogen column integrated along the line of sight. A velocity analysis of the neutral gas allows one to separate the different galactic components on the light of sight (Figure 5). Following the Fountain et al. (1983) results based on a Hα study of the NAN, the LSR velocity of the nebula is -7.1 ± 5.5 km s^{-1} with a FWHM of 28.6 ± 0.6 km s^{-1}. The fraction of HI emission coming from this velocity range represents $40 \pm 7\%$ of the total. This value is an upper limit since not all the gas in this velocity range is associated with the complex. For $[N({\rm HI}) + N({\rm H_2})]/A_V = 1.87 \times 10^{21}$ (Savage & Mathis 1979) the upper limit for the visual extinction in the reference field is about 0.78 ± 0.14 mag (only 0.4% is associated with the molecular gas).

Star count method

The extinction is derived from K_s counts as described in § 2.1. Once the color map has been calibrated (previous paragraph), the star count extinction map is adjusted using a linear relation for the zero point versus the galactic latitude and longitude. For the NAN area, the stellar density is found to increase by $\sim 25\%$ per degree toward the galactic plane. The cell size is allowed to vary to achieve the desired number of stars, 10 in this work. Since the $H - K_s$ intrinsic color dispersion is low, this small number gives good results for the color

map ($\sigma(A_V) = 1.9/\sqrt{10} = 0.6$ mag). However, this small number introduces a significant Poisson noise in the star count map in which the standard deviation of the extinction is $\sigma = 3.5$ mag. For $A_V \gtrsim 20$ mag, the uncertainty is actually reduced for K_s star counts because the cell size is constrained by the H band which is more sensitive to extinction. Cells in high extinction regions contain 10 stars simultaneously detected in H and K_s and more than 10 additional stars detected only in K_s. The statistical uncertainty in the K_s star count map is reduced to $\sigma \approx 2.5$ mag when $A_V \gtrsim 20$ mag.

Foreground star density estimation

Figure 6 shows the extinction from star counts and from reddening in the most obscured portion of the field. The effect of the foreground star contamination is obvious: the extinction derived from star counts reaches 30 mag where the extinction derived from reddening drops suddenly to 0 mag. In areas where $A_V(\text{starcounts}) - A_V(\text{color}) > 20$ (i.e. 5.5σ) we find 57 stars. Among them, we identify 15 stars which do not show any $J - K_s$ excess (the expected excess when $A_V = 20$ is $E_{J-K_s} = 3.4$). The normalized density for this foreground star population corresponds to 1900 ± 500 stars deg^{-2} and represents $\sim 6\%$ of the total star number for an unobscured field.

Foreground star correction

Unfortunately, setting a color threshold to separate the two star populations systematically yields a foreground star distribution that is strongly correlated with the dust distribution. The degeneracy between background blue stars and foreground red stars prevents the proper separation of the two populations. To correct for the foreground star contamination, we remove the 30 bluer (i.e. lower $J-K_s$) stars per $7.5' \times 7.5'$ box in the whole field, corresponding to the foreground star density measured toward the densest part of the cloud. In high extinction regions this procedure removes foreground stars, but for visual extinction lower than ~ 15 mag the degeneracy prevents a correct separation of the two populations and a bias is introduced in the extinction maps. The resulting foreground star distribution is presented in Figure 7. The iteration of the star counts and the reddening analysis with the new version of the catalog provides the foreground star corrected extinction maps (Figure 8). The standard deviation of the difference between these maps and maps obtained before the foreground star correction are 0.1 and 0.9 mag for the color and the star count extinction map, respectively. The main difference comes from the cloud core which corresponds to a high extinction for both maps: visual extinction is larger than 25 mag in the color map where it was 0 mag before the correction.

To estimate the error in the foreground star correction we compare the distribution of these stars with the dust distribution. The difference between the mean extinction in the whole field and the mean value measured at the position of each supposedly foreground star should give zero for uncorrelated distributions. We find $\Delta A_V = -0.26$ mag. Simulations for an uniformly distributed star field yield a standard deviation of $\sigma = 0.03$. The spatial distribution of the selected stars is still correlated with the extinction and is therefore not consistent with a population of only foreground stars. The fraction of foreground stars in a $7.5' \times 7.5'$ box reaches 0.5 for the darkest region and is less than 0.1 for $A_V \lesssim 15$. Consequently, in regions for which the stellar color degeneracy exists, fewer than 10% of the stars are affected by the selection bias. For higher values, the foreground star identification is straightforward (i.e. not statistical). We conclude that the contamination by residual background stars in the sample has negligible consequences on the extinction mapping compared to the intrinsic dispersion of these maps: the standard deviation between the corrected and the not-corrected maps are 0.1 and 0.9 mag whereas the intrinsic uncertainty for the extinction maps are $\sigma = 0.6$ and $\sigma = 3.5$ mag for the color and the star count map, respectively.

Merging the two maps

The uncertainty is lower from the color analysis than for star counts for $A_V < 15$. For higher values, it is not clear whether star counts or color give the best answer. The color method is more constraining because of the necessity to detect stars in both H and K_s bands whereas only detections in K_s are required to build the star count map. Since stars are detected only in the longer wavelength in the most extinguished areas, more data are available for the star counts than for the color analysis. Statistical uncertainties are lower in the star count map when the number of K_s stars is greater than 300 in a cell (that by construction always contains 10 stars detected in both H and K_s). Using the extinction law, the mean color $\overline{H - K_s} = 0.16 \pm 0.01$ and the limiting magnitude difference for each band, $H^{\rm lim} - K_s^{\rm lim} = 0.5$ mag, it would correspond to $A_V \approx 70$ mag. *Therefore, the color analysis technique has a lower statistical uncertainty everywhere in our field.*

The resolution of the extinction maps is adapted to the local star density. It is $1.2'$ for $A_V = 0$ mag, $1.9'$ for $A_V = 10$ mag, $3.7'$ for $A_V = 20$ mag and $7'$ for $A_V > 30$ mag. Unfortunately, extinction is probably no longer homogeneous for resolutions coarser than 0.5 pc ($3'$ for $d = 580$ pc) and both methods underestimate the extinction in a non-linear way. This effect can be simulated using an uniform spatial distribution for the stars and a the luminosity functions observed with 2MASS toward the NAN direction (see figure 2). One can then redden this simulated stellar field with any known extinction profile, assuming

all stars are background and applying the 2MASS completeness cuts. The simulation of a Gaussian peak of 30 mag of visual extinction with a 50″ FWHM observed at 100″ resolution gives $A_V(H-K_s) = 4.6$ mag and $A_V(K_s\,\mathrm{counts}) = 8.0$ mag. A 90″ Gaussian peak observed at a 100″ resolution gives $A_V(H-K_s) = 16.5$ mag and $A_V(K_S\,\mathrm{counts}) = 18.8$ mag. When the extinction is not homogeneous over a cell, star counts lead to a higher value than reddening. But both methods underestimate the peak value. Thus, at the highest extinctions, using these techniques at the 2MASS sensitivity underestimates the extinction. Deeper observations are needed such as those presented in Alves et al. (2001) with limiting magnitudes of about 20 mag in both H and K_s.

Our analysis concludes that (1) the color method is more robust than stars counts to the foreground star contamination. This contamination can be corrected by comparing color and count maps. (2) The star count extinction map has larger statistical uncertainty than the color extinction map. (3) The star count analysis is more robust than the color analysis to extinction inhomogeneities within a cell, i.e. the systematic uncertainty is smaller in the star count map for high extinction. Because of these different characteristics, we decided to combine the two extinction maps using reddening for $A_V < 15$, star counts for $A_V > 25$ and a linear combination of the two maps for the intermediate extinction range:

$$A_V = x \times A_V(K_s\,\mathrm{counts}) + (1-x) \times A_V(H-K_s) \tag{8}$$

where:

$$\begin{array}{lll} x = 0 & \text{for} & A_V(K_s\,\mathrm{counts}) < 15 \\ x = \left[A_V(K_s\,\mathrm{counts}) - 15\right]/10 & \text{for} & 15 \leq A_V(K_s\,\mathrm{counts}) < 25 \\ x = 1 & \text{for} & A_V(K_s\,\mathrm{counts}) \geq 25 \end{array}$$

The final combined extinction map of the NAN is presented in Figure 9. The maximum visual extinction is $A_V = 35$ mag whereas previous works at optical wavelengths estimate the extinction to less than 10 mag (Goudis & White 1979; Straižys et al. 1993). The 2MASS near–infrared data allow deeper analysis of the dust distribution.

Cloud mass

The cloud mass is derived from the extinction map using the following relation (Dickman 1978):

$$M = (\alpha d)^2\, \mu\, \frac{N_H}{A_V} \sum_i A_V(i) \tag{9}$$

where α is the angular size of a pixel map, d the distance to the cloud, μ the mean molecular weight corrected for the helium abundance, and i represents a pixel map. With the dust-to-gas proposed by Savage & Mathis (1979), $N_H/A_V = 1.87 \times 10^{21}$ cm^{-2} mag^{-1} (N_H =

$N_{HI} + N_{H_2}$) and a distance of 580 pc, we obtain a mass of 4.5×10^4 $M_\odot$. This value corresponds to about one fifth of the Orion cloud mass (Maddalena et al. 1986; Cambrésy 1999). Uncertainties come from the distance estimate for the cloud and the systematic error in the extinction. An uncertainty of a factor of two is believed to be a reasonable estimate. Figure 10 shows how the integrated mass distribution varies with the extinction within the cloud. Regions with visual extinction greater then 20 mag account for less than 3% of the total mass of the cloud. This suggests that the underestimation of the extinction in the cloud cores has only a limited consequence on the total mass estimate.

Bally & Scoville (1980) estimated the molecular cloud mass from CO observation to 3-6 $\times 10^4$ $M_\odot$ for a distance of 1 kpc. For 580 pc, it would correspond to 1-2 $\times 10^4$ $M_\odot$. The discrepancy might come from the N_H/A_V value or from the conversion of CO density to H_2 density.

3.3.2. Limitations of the method

The cloud distance is the most critical parameter in the accurate application of these methods. The farther away a cloud, the lower is the spatial resolution and the larger the number of foreground stars. Here, we have mapped visual extinctions of 15 mag at a resolution of $3'$ which corresponds to 0.5 pc (d = 580 pc). If the cloud were at 2 kpc, the $3'$ resolution would correspond to 1.7 pc, equivalent to a study of nearby clouds such as Taurus, Chamaeleon or ρ Ophiuchus at a $40'$ angular resolution. This is the resolution of DIRBE/COBE and is probably close to the *minimum acceptable* to derive properties within a cloud. As the distance increases the number of foreground stars increases, as well, further degrading extinction maps.

The 2MASS star density is about 4 times higher toward the galactic center than for the NAN direction. Clouds toward such very high density directions could therefore be mapped with a better resolution for a same distance. In contrast, the star density is about 3.5 times lower toward the anti-center and dramatically decreases for higher galactic latitudes (density divided by 2 at $b \approx 5°$). Thus, the maximum distance for which molecular clouds can be mapped using 2MASS with this method cannot exceed 3 kpc toward very high density directions such as toward the galactic bulge.

3.3.3. Star Formation

The technique described in section 2.3.2 allows one to identify star clusters by combining the color and the star count extinction maps. Since a cluster is an excess of stars compared to the local density, it should appear as a deficit of extinction in the star count map compared to the color map. To identify star clusters toward the NAN, we select areas for which $A_V(\mathrm{color}) - A_V(\mathrm{counts}) > 6 \approx 1.7\sigma$ and that contain two adjacent pixels with $A_V(\mathrm{color}) - A_V(\mathrm{counts}) > 14 \approx 4.0\sigma$. These numbers were chosen subjectively after examination of the full resolution 2MASS images. Nine cluster identifications are proposed in Table 1, and Figure 11 shows their position in the cloud. Figure 12 shows the 2MASS color images with the threshold contour overlaid. Among these nine clusters, only number 3b and 7 were already known (Herbig 1958; Wendker et al. 1983, respectively).

Cluster 1 and 2. They are located on the edge of the central core of the dark cloud. The low density clustering of these red stars suggests either that the star formation occurs in the whole core (they are detected on the edge because the extinction is lower and the projection effect helps the detection at these locations) or that they are in the process of being dispersed. An upper limit for the star density excess can be obtained by assuming that the color map gives the *true* extinction and that the star counts underestimate the extinction because of the clustering. This yields only an upper limit because young stars are known to have an intrinsic infrared excess. For clusters 1 and 2 we find that the contour overlaid in Figure 12 corresponds to an excess of ~ 4 arcmin^{-2} and that the density reaches a maximum of ~ 20 arcmin^{-2} in their center. For comparison, clusters 5 and 6 have a similar value for the lowest contour but they both reach a maximum density 4 times larger of about 80 arcmin^{-2}.

Clusters 3a and 3b. These two clusters are on the edge of the same globule. 3a contains faint red stars and 3b bright blue objects. Their relative position within the cloud may explain these colors (3a on the front side and 3b on the back side of the cloud). 3b was discovered by Herbig (1958).

Cluster 4. It is located in a low extinction area and stars do not exhibit any infrared excess. It not clear whether this cluster is associated with the dark cloud; it might be a more distant open cluster.

Clusters 5 and 6. These are the two most obvious clusters from the star count and color comparison with $A_V(\text{color}) - A_V(\text{starcount}) > 25$ mag. They both lie on the edge of a highly extinguished globule. Cluster 6 is associated with an emission nebula that strongly supports the hypothesis of association with the cloud.

Clusters 7 and 8. These are in the North America nebula (in the HII region), in a low extinction area ($A_V \approx 3$ mag) and apparently not associated with any extinction core. The clustering is obvious for both clusters but there is no other proof of their association with the dark cloud at 580 pc. Cluster 7 has been observed by Wendker et al. (1983) who concluded it is located in the Perseus spiral arm, at a kinematic distance of 5-7 kpc, far behind the NAN. Cluster 8 is very compact compared to the others and that might indicate a larger distance. It contains 12 stars among which 3 are detected in JHK_s, 3 in HK_s and 6 in K_s only.

4. Conclusion

We have proposed a method to map extinction with 2MASS data using simultaneously K_s star counts and $H - K_s$ reddening. Finding a value of the extinction significantly larger from the count map than from the color map indicates significant foreground star contamination. Foreground stars can be removed individually in high extinction regions and statistically elsewhere. We stress the point that the foreground population dominates for high extinction and these regions would not be correctly analyzed if foreground stars are not carefully removed. On the other hand, a higher extinction value derived from colors than from counts indicates the presence of a star cluster. The adaptive method increases the angular resolution of the mapping around these objects. Color, especially $H - K_s$, is generally a better estimator of the extinction than star counts which have a higher statistical uncertainty.

Towards the NAN, we estimate the foreground star density to 1900 ± 500 stars deg^{-2} and the visual extinction is mapped up to 35 mag. Angular resolution of the extinction map depends on the local stellar density and is $1.2'$, $3.7'$ and $7'$ for visual extinctions of about 0, 20 and > 30 mag, respectively. Nine clusters are identified, only two of which were already known and another two of which correspond to a diffuse excess of red stars close the center of the cloud, suggesting an *evolved* young population or star forming activity in the whole core (~ 5 pc diameter).

Near-infrared wavelengths are required to investigate such highly obscured fields. With

the help of the accurate 2MASS photometry, we have obtained results that supersede the previous work on the extinction in this area. The method developed here can be extended to other high extinction clouds with a significant fraction of foreground stars (i.e. located at more than 500 pc, in the galactic plane) that were not accessible before. The knowledge of the extinction toward the galactic plane is essential in order to constrain stellar population model parameters, such as the diffuse extinction and the giant star distribution, that are not well constrained at higher galactic latitudes (see appendix). The generalization of studies based on the comparison of the extinction (derived from star counts and color) with molecular lines and/or far–infrared and submillimeter emission is now possible with the 2MASS data releases.

This publication makes use of data products from the Two Micron All Sky Survey, which is a joint project of the University of Massachusetts and the Infrared Processing and Analysis Center/California Institute of Technology, funded by the National Aeronautics and Space Administration and the National Science Foundation.

L. Cambrésy acknowledges partial support from the Lavoisier grant of the French Ministry of Foreign Affairs.

A. Comparison with a galactic stellar distribution model

The extinction calibration is based on the $H - K_s$ color in the reference field. This field is assumed to be representative of the aggregate color over the field containing the NAN. Deviations from this color are interpreted as extinction from the dust associated with the complex. To validate this procedure, we have compared the 2MASS star counts with the predicted counts based on galactic stellar distribution model, which predicts both the star counts and general interstellar medium extinction for the region of the Milky Way that includes the NAN. After incorporating the derived NAN extinction map with the model star counts, the extincted star counts should match the observed 2MASS star counts (§ A.3).

A.1. The Model

The genesis of stellar distribution model comes from the Bahcall & Soneira (1980) optical star count model. Jarrett (1992) modified the Bahcall & Soneira model using the discrete formalism of Elias (1978), Jones et al. (1981) and Garwood & Jones (1987), extending the model to the near-infrared (1-5 μm). The model includes the class III evolved giants, class

IV subdwarfs, class V main sequence, brown dwarfs (types L and T), and AGB populations. As with the Bahcall & Soneira model, the stars are distributed in two primary large-scale components: disk (exponential profile) and spheroid ($R^{1/4}$ profile). Colors, luminosity, and number density per spectral type are based on the empirical data from Wielen (1974), Wielen et al. (1983), Koornneef (1983), Reid & Gilmore (1982), Hawkins & Bessell (1988), Bessell (1990), Bessell & Brett (1988). The interstellar extinction is applied as a smooth exponential function of galactic position, characterized by its own scale height and disk length. In total there are several adjustable parameters, including disk/spheroid scale lengths, scale heights, luminosity function and dispersion, and extinction/reddening laws. The model parameters were tuned using deep optical and infrared star counts (see below).

A.2. Validation of the Model

The optical portion of the model was *tuned* and validated using deep CCD observations, $V < 24$ mag, $R < 22$ mag, of a diverse set of fields, encompassing both low and high stellar number density (Jarrett 1992; Jarrett et al. 1994). The near-infrared portion was tuned and validated using 2MASS star counts, for $J < 15.5$ and $K_s < 14$ mag, for fields ranging from $0° < |b| < 90°$ (Table 2). The typical field size was 25 deg^2. The model performs well for $|b| > 20°$. An illustrative example of the performance for $l = 90°$ $b = 30°$ is given in Figure 13. At low galactic latitudes the model has small but significant differences compared with 2MASS, probably due to differential extinction from clouds along the line of sight (e.g., see $|b| < 5°$ in Table 2, corresponding to regions of the plane that are in close proximity to the NAN). A direct comparison with the NAN is given in § A.3.

A.3. Comparing the model with the 2MASS NAN observations

The galactic stellar distribution model adequately ($\sim$ 10-20%) predicts the number density and colors of stars located in the galactic plane, including areas near the NAN (Table 2). For the cloud itself, an additional source of extinction is required to match the model with 2MASS measurements. The histogram of the extinction we obtained using our extinction map allows us to redden statistically stars that are located more than 580 pc from the Sun (the nominal NAN cloud distance). We emphasize that this extinction component (attributed to the NAN cloud) is an addition to the nominal interstellar extinction component that is built into the model (§ A.1).

Figure 14 compares the 2MASS data with the extincted-corrected model predictions.

The upper panels show the results for the cloud complex ($l = 85°$, $b = -0.9°$) and the lower panels show the results for the reference field ($l = 86.2°$, $b = -2.9°$). The lower left panel shows differential star counts for the reference region, where the solid and dashed lines correspond to the model and the diamonds denote the 2MASS measurements. Note that the evolved stars dominate the bright end ($K_s < 11$ mag) and disk dwarfs dominate the faint end. The $H - K_s$ color histograms are shown in the lower right panel for the reference region. Both the star counts and colors suggest that the 2MASS measurements are well fitted by the model predictions (see also Table 2). The upper left panel shows the differential star counts for the region along the cloud line-of-sight. The shape of the $H - K_s$ color histograms are remarkably similar (right upper panel), again suggesting that the model+cloud extinction adequately describes the stellar distribution toward the NAN. For comparison we show (upper right hand panel) the predicted stellar colors for stars located along the line-of-sight that is directly opposite the NAN in the galactic plane (i.e., $l = 85°$, $b = +0.9°$; see Table 2). Here we have applied an ad hoc extinction, $A_V = 1$ mag at 4 kpc, to match the 2MASS star counts along this line of sight (Table 2, note (c)). This is consistent with the expected low extinction derived from CO emission along this line of sight with $W(\mathrm{CO}) = 11.08$ K km s^{-1} (Dame et al. 2001) which corresponds to $A_V = 1.1$ mag. Star colors are relatively bluer and the total number of sources is nearly double to what is seen toward the NAN.

The star count model suggests that the extinction in the reference region is probably quite small, consistent with HI observations and visual inspection of the POSS plates. Moreover, the predicted number of foreground stars, 1900 ± 500 deg^2, implies a cloud distance, ~ 485 pc, that is comparable (within the model uncertainties, ~ 100 pc) to the currently accepted distance to the NAN, ~ 580 pc. Given the overall high-quality consistency between the model predictions and the 2MASS measurements, we conclude that the reference field gives the correct zero point color in the whole NAN complex, and the derived extinction map is a fair representative of the dust column density attributed to the NAN.

Table 1. Coordinates Of The Star Clusters

Id	R.A. (J2000)	Dec. (J2000)
1	20 56 02	43 37 00
2	20 57 12	43 48 30
3a	20 58 28	43 56 24
3b	20 58 19	43 53 37
4	20 56 13	44 23 05
5	20 50 50	44 25 00
6	20 53 42	44 31 36
7	20 53 35	44 47 20
8	20 54 14	44 54 07

Table 2. 2MASS Fields Used To Constrain Model Parameters

$l(^\circ)$	$b(^\circ)$	note	Performances	
			star counts	color
90	90	Galactic North Pole	nominal	nominal
90	50		nominal	nominal
90	30		nominal	nominal
90	20		nominal	(a)
270	20		nominal	nominal
90	15		nominal	(a)
90	10		(b)	(a)
180	10	Galactic Anticenter	nominal	nominal
270	10		nominal	nominal
90	5		(b)	(a)
90	2		nominal	(a)
86	-2.9	reference field (Fig. 14, lower panels)	nominal	nominal
85	1	opposite the NAN	(c)	(c)

Note. — *Star counts* refer to counts at $K_s = 14^{\rm th}$ mag; *colors* refer to the $J-H$, $H-K_s$ and $J-K_s$ mag differences. A *nominal* result means that the model star counts are within 10% of the 2MASS star counts. (a): slight color excess in the 2MASS $J-K_s$ with respect to the model colors. (b): 2MASS K_s-band star counts in $\sim 20\%$ excess with respect to the model. (c): star counts and colors are nominal only if an additional (ad hoc) source of extinction is included in the model: $A_V = 1.0$ at 4 kpc.

REFERENCES

Alves, J., Lada, C. J., & Lada, E. A. 2001, Nature, 409, 159

Alves, J., Lada, C. J., Lada, E. A., Kenyon, S. J., & Phelps, R. 1998, ApJ, 506, 292

Andreazza, C. M. & Vilas-Boas, J. W. S. 1996, A&AS, 116, 21

Bahcall, J. N. & Soneira, R. M. 1980, ApJS, 44, 73

Bally, J. & Scoville, N. Z. 1980, ApJ, 239, 121

Beichman, C. A. & Jarrett, T. 1994, Ap&SS, 217, 207

Bessell, M. S. 1990, PASP, 102, 1181

Bessell, M. S. & Brett, J. M. 1988, PASP, 100, 1134

Bok, B. J. 1956, AJ, 61, 309

Burton, W. B. & Hartmann, D. 1994, in ASP Conf. Ser. 67: Unveiling Large-Scale Structures Behind the Milky Way

Cambrésy, L. 1999, A&A, 345, 965

Cambrésy, L., Epchtein, N., Copet, E., de Batz, B., Kimeswenger, S., Le Bertre, T., Rouan, D., & Tiphène, D. 1997, A&A, 324, L5

Cardelli, J. A., Clayton, G. C., & Mathis, J. S. 1989, ApJ, 345, 245

Carpenter, J. M. 2000, AJ, 120, 3139

Cernicharo, J. & Bachiller, R. 1984, A&AS, 58, 327

Cutri, R. M., Skrutskie, M. F., Van Dyk, S., Chester, T., Evans, T., Fowler, J., Gizis, J., Howard, E., et al. 2000, Explanatory Supplement to the 2MASS Second Incremental Data Release

Dame, T. M., Hartmann, D., & Thaddeus, P. 2001, ApJ, 547, 792

Della Prugna, F., Calvet, N., & Araque, M. D. C. 1984, Revista Mexicana de Astronomia y Astrofisica, 9, 31

Dickman, R. L. 1978, AJ, 83, 363

Elias, J. H. 1978, ApJ, 223, 859

Epchtein, N. 1997, in The Impact of Large Scale Near–Infrared Sky Surveys, eds. F. Garzón, N. Epchtein, A. Omont, B. Burton, & P. Persi (Tenerife: Kluwer Academic Publishers)

Feldt, C. & Wendker, H. J. 1993, A&AS, 100, 287

Fountain, W. F., Gary, G. A., & O'Dell, C. R. 1983, ApJ, 269, 164

Frerking, M. A., Langer, W. D., & Wilson, R. W. 1982, ApJ, 262, 590

Garwood, R. & Jones, T. 1987, PASP, 99, 453

Goudis, C. & White, N. J. 1979, A&A, 78, 373

Gregorio Hetem, J. C., Sanzovo, G. C., & Lépine, J. R. D. 1988, A&AS, 76, 347

Hawkins, M. R. S. & Bessell, M. S. 1988, MNRAS, 234, 177

Herbig, G. H. 1958, ApJ, 128, 259

Jarrett, T. H. 1992, An optical study of the faint end of the stellar luminosity function, Ph.D. thesis, Massachusetts Univ., Amherst.

Jarrett, T. H., Dickman, R. L., & Herbst, W. 1994, ApJ, 424, 852

Jones, T. J., Ashley, M., Hyland, A. R., & Ruelas-Mayorga, A. 1981, MNRAS, 197, 413

Jones, T. J., Hyland, A. R., & Bailey, J. 1984, ApJ, 282, 675

Koornneef, J. 1983, A&A, 128, 84

Kramer, C., Alves, J., Lada, C. J., Lada, E. A., Sievers, A., Ungerechts, H., & Walmsley, C. M. 1999, A&A, 342, 257

Lada, C. J., Alves, J., & Lada, E. A. 1999, ApJ, 512, 250

Lada, C. J., Lada, E. A., Clemens, D. P., & Bally, J. 1994, ApJ, 429, 694

Lynds, B. T. 1962, ApJS, 7, 1

Maddalena, R. J., Morris, M., Moscowitz, J., & Thaddeus, P. 1986, ApJ, 303, 375

Marcy, G. W. 1980, AJ, 85, 230

Mattila, K. 1986, A&A, 160, 157

Padoan, P., Jones, B. J. T., & Nordlund, A. P. 1997a, ApJ, 474, 730

Padoan, P., Nordlund, A., & Jones, B. J. T. 1997b, MNRAS, 288, 145

Reid, N. & Gilmore, G. 1982, MNRAS, 201, 73

Rieke, G. H. & Lebofsky, M. J. 1985, ApJ, 288, 618

Rossano, G. S. 1980, AJ, 85, 1218

Savage, B. D. & Mathis, J. S. 1979, ARA&A, 17, 73

Schultheis, M., Ganesh, S., Simon, G., Omont, A., Alard, C., Borsenberger, J., Copet, E., Epchtein, N., et al. 1999, A&A, 349, L69

Stepnik, B., Abergel, A., Bernard, J.-P., Boulanger, F., Cambrésy, L., Giard, M., Jones, A., Lamarre, J.-M., et al. 2001, A&A, in press

Straižys, V., Kazlauskas, A., Vansevičius, V., & Černis, K. 1993, Baltic Astronomy, 2, 171

Thoraval, S., Boissé, P., & Duvert, G. 1997, A&A, 319, 948

Welin, G. 1973, A&AS, 9, 183

Wendker, H. J., Baars, J. W. M., & Benz, D. 1983, A&A, 124, 116

Westerhout, G. 1958, Bull. Astron. Inst. Netherlands, 14, 215

Wielen, R. 1974, Highlights in Astronomy, 3, 395

Wielen, R., Jahreiß, H., & Krüger, R. 1983, in IAU Colloq. 76: Nearby Stars and the Stellar Luminosity Function

Wolf, M. 1923, Astron. Nachr., 219, 109

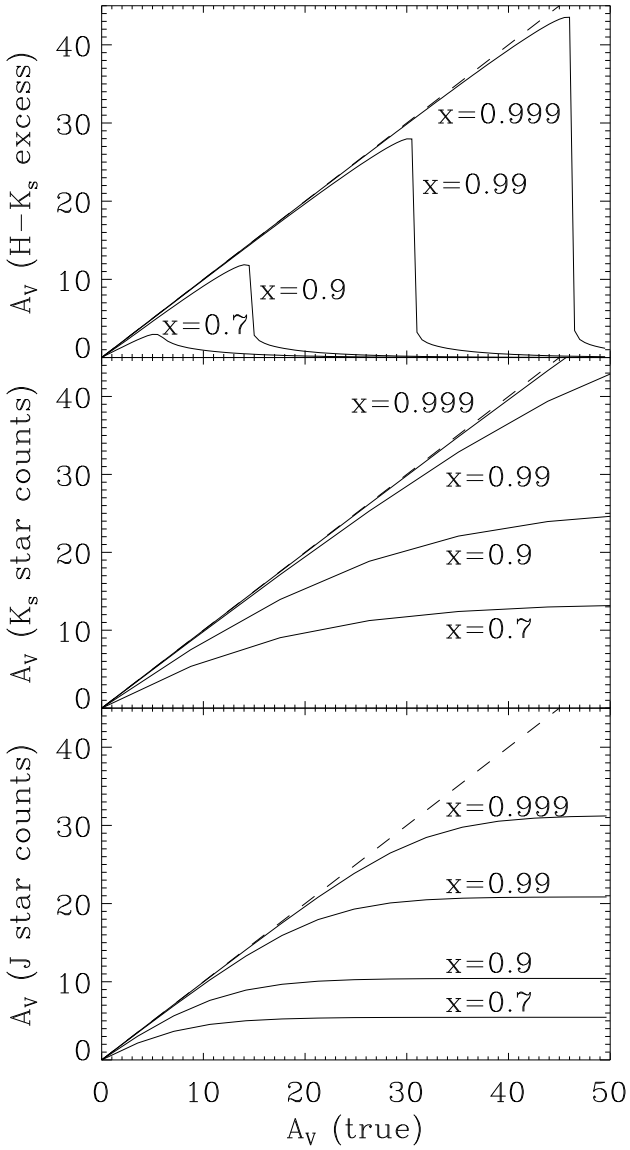

Fig. 1.— Effect of the foreground star contamination on the *measured* extinction versus the *true* extinction for different degree of contamination ($X = N^{\rm background}/N^{\rm total}$) and different methods ($H - K_s$ color, K_s star counts and J star counts).

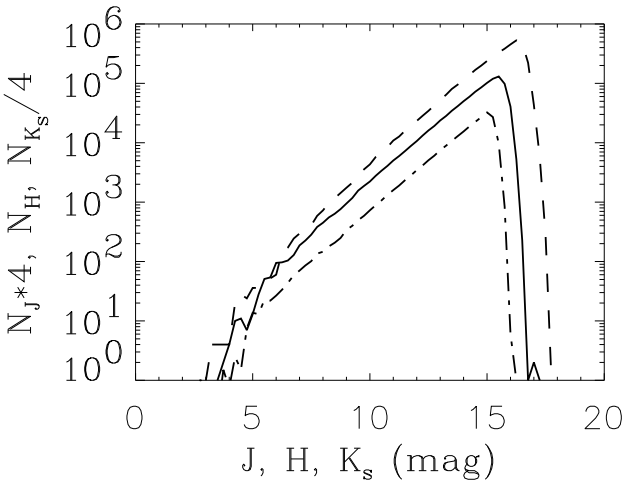

Fig. 2.— Histogram distribution of the 2MASS magnitudes in the NAN (J: dashed line, H: solid line and K_s: dashed-dotted line). Slopes of the luminosity functions are 0.36, 0.34 and 0.34 for J, H and K_s, respectively.

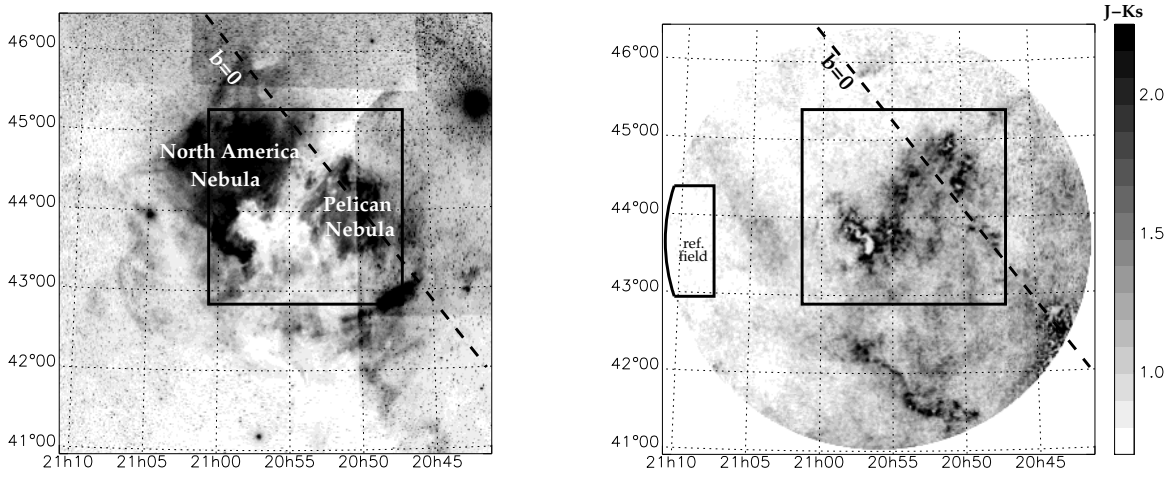

Fig. 3.— Digitized Sky Survey optical image (left) and 2MASS $J - K_s$ map (right) of the NAN. The square shows the area studied in the paper. The reference field is used to set the zero point of extinction. Coordinates are expressed in the equatorial J2000 system.

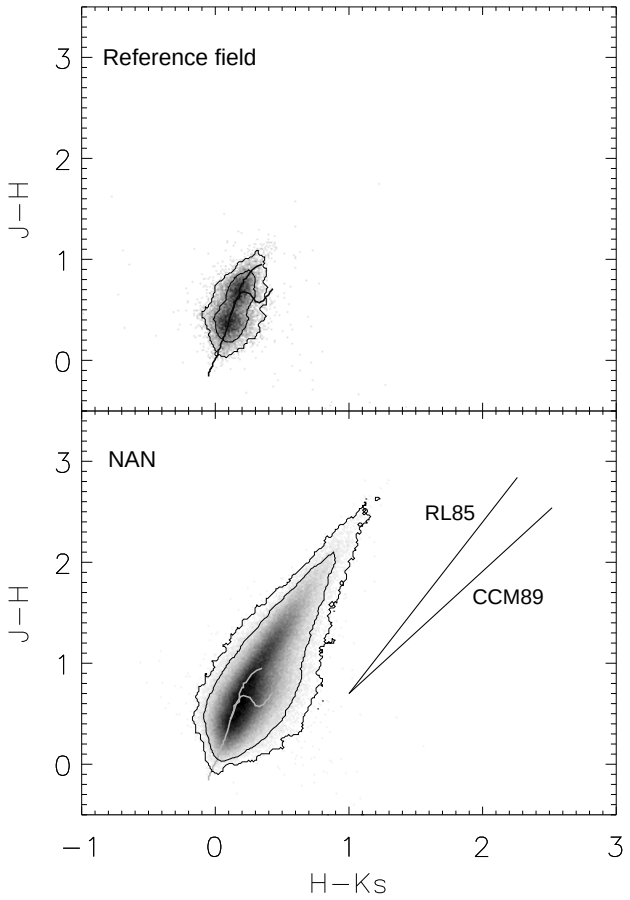

Fig. 4.— Color color diagram for the reference field (top) and the NAN (bottom) directions. RL85 and CCM89 are the reddening vectors for Rieke & Lebofsky (1985) and Cardelli et al. (1989) extinction laws, respectively. Dwarf and giant sequences are overlaid (Bessell & Brett 1988).

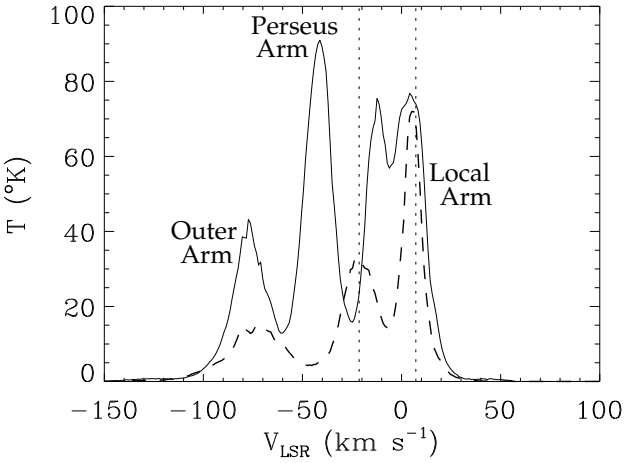

Fig. 5.— Velocity components toward the NAN (solid line) and the reference field (dashed line) from the Leiden/Dwingeloo survey. The vertical dotted lines show the velocity range of the NAN (in the Local Arm).

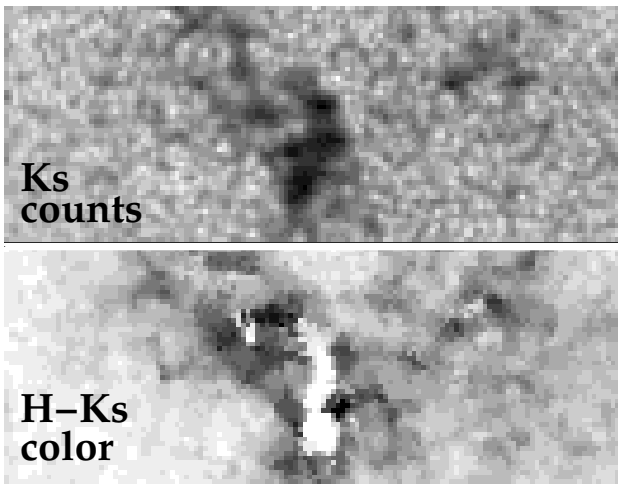

Fig. 6.— Extinction maps from K_s star counts (top) and $H - K_s$ color (bottom) for a $64' \times 24'$ field centered on the most obscured region of the dark cloud ($\alpha_{\rm J2000} = 20^{\rm h}56^{\rm m}51^{\rm s}$, $\delta_{\rm J2000} = 43°42^{\rm m}33^{\rm s}$). Black is for high extinction and white for low extinction. Extinction from star counts reaches 30 mag whereas the extinction from reddening at the same position is 0 mag due to the foreground star contamination (see § 2.3.2).

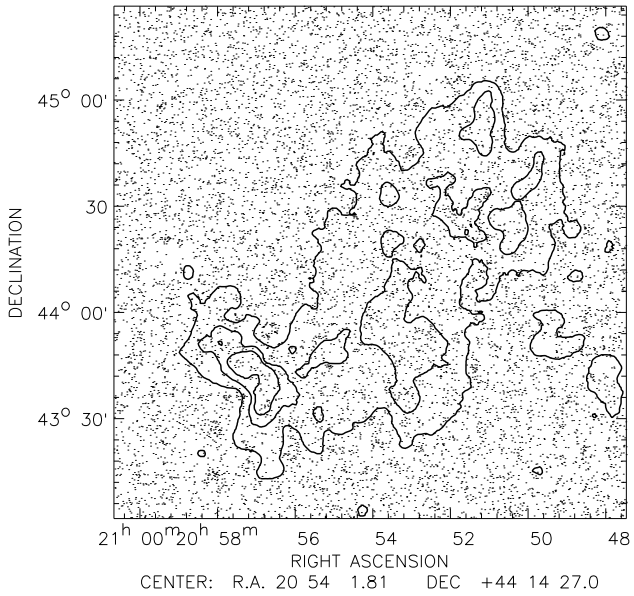

Fig. 7.— Distribution of foreground stars with smoothed extinction contours overlaid (contour values are 5, 10 and 15 A_V). Extinction is derived from $H - K_s$ color.

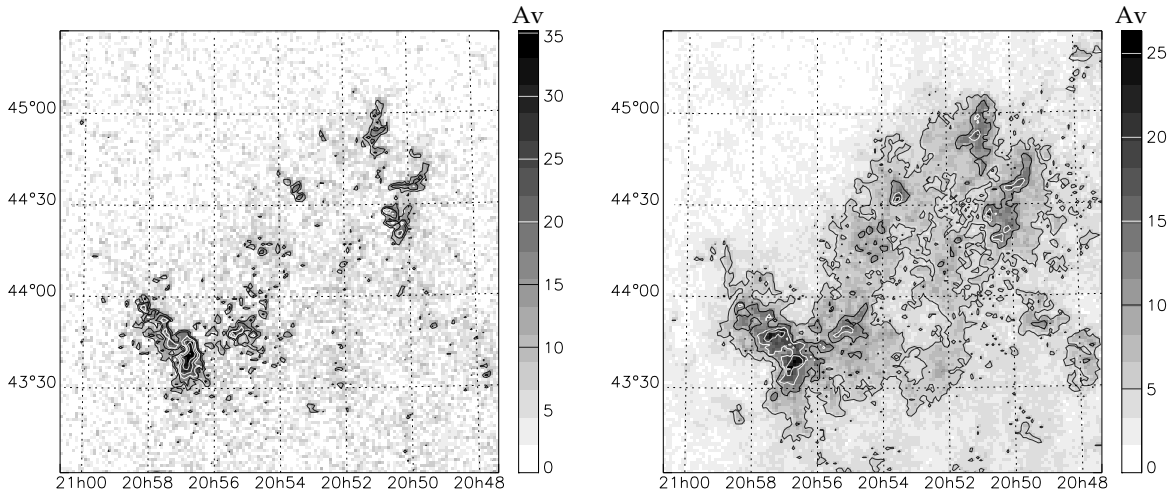

Fig. 8.— Extinction maps derived from K_s star counts (left) and from $H - K_s$ color (right) corrected for foreground stars. Coordinates are expressed in the equatorial J2000 system.

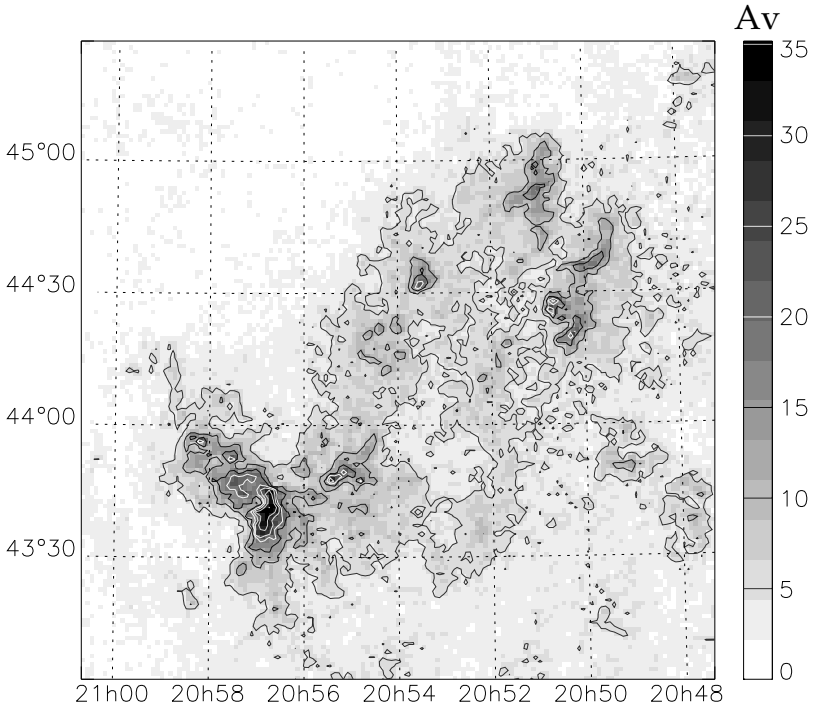

Fig. 9.— Extinction map of the NAN obtained by combination of the $H - K_s$ color map with the K_s star count map.

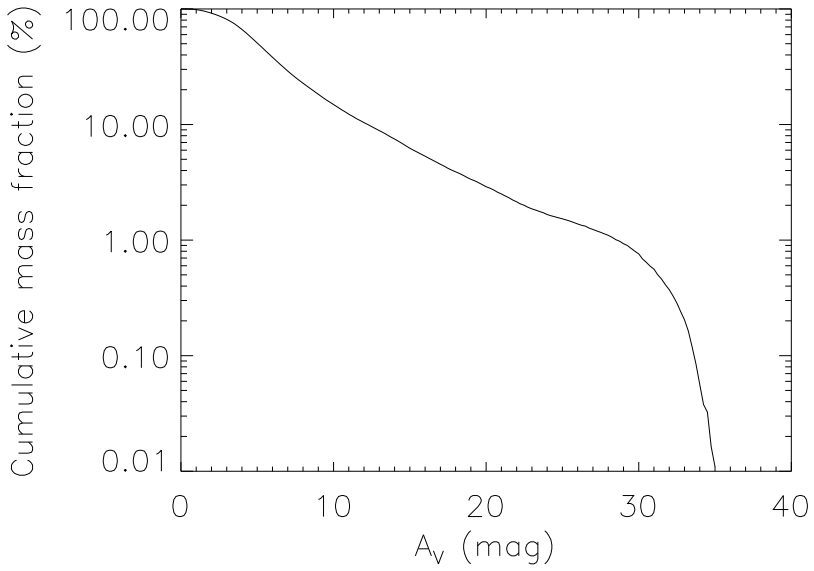

Fig. 10.— Cumulative enclosed mass in iso-extinction contours versus visual extinction.

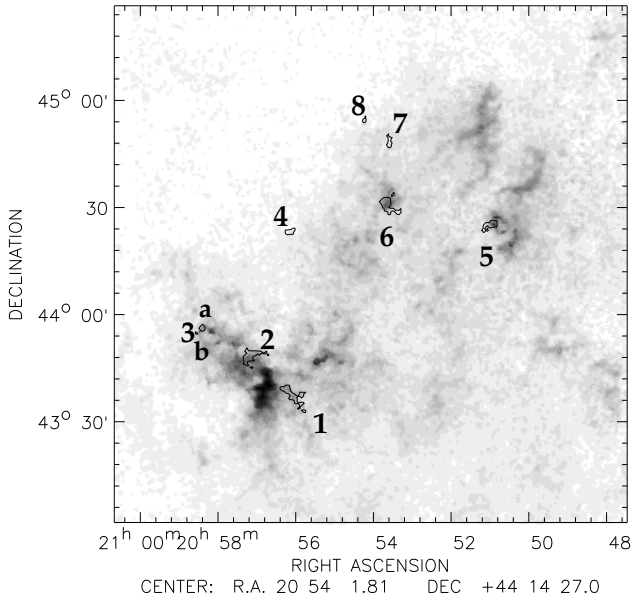

Fig. 11.— Position of the nine clusters (contours correspond to $A_V(\mathrm{color}) - A_V(\mathrm{counts}) > 6$ mag) represented on the combined extinction map of the cloud.

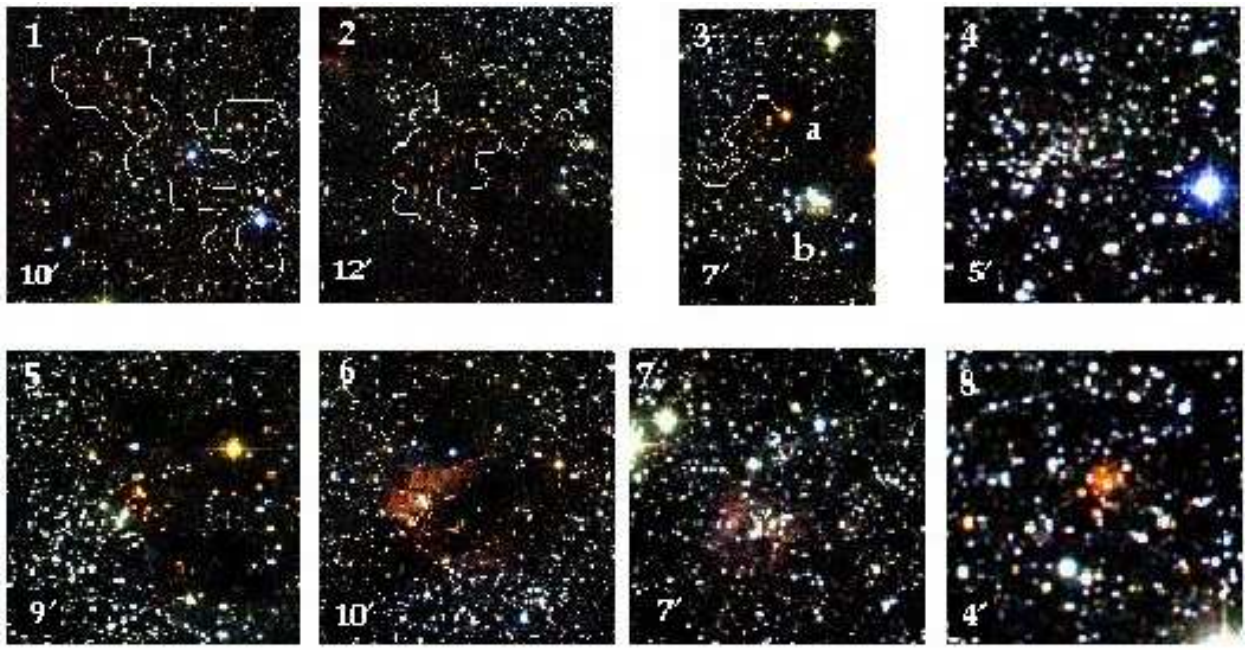

Fig. 12.— JHK_s color images of the clusters selected by comparison of the local stellar density with the median reddening. The width of each field is specified in the lower left corner. Contour for $A_V(\mathrm{color}) - A_V(\mathrm{counts}) > 6$ mag is overlaid when the clustering is not obvious.

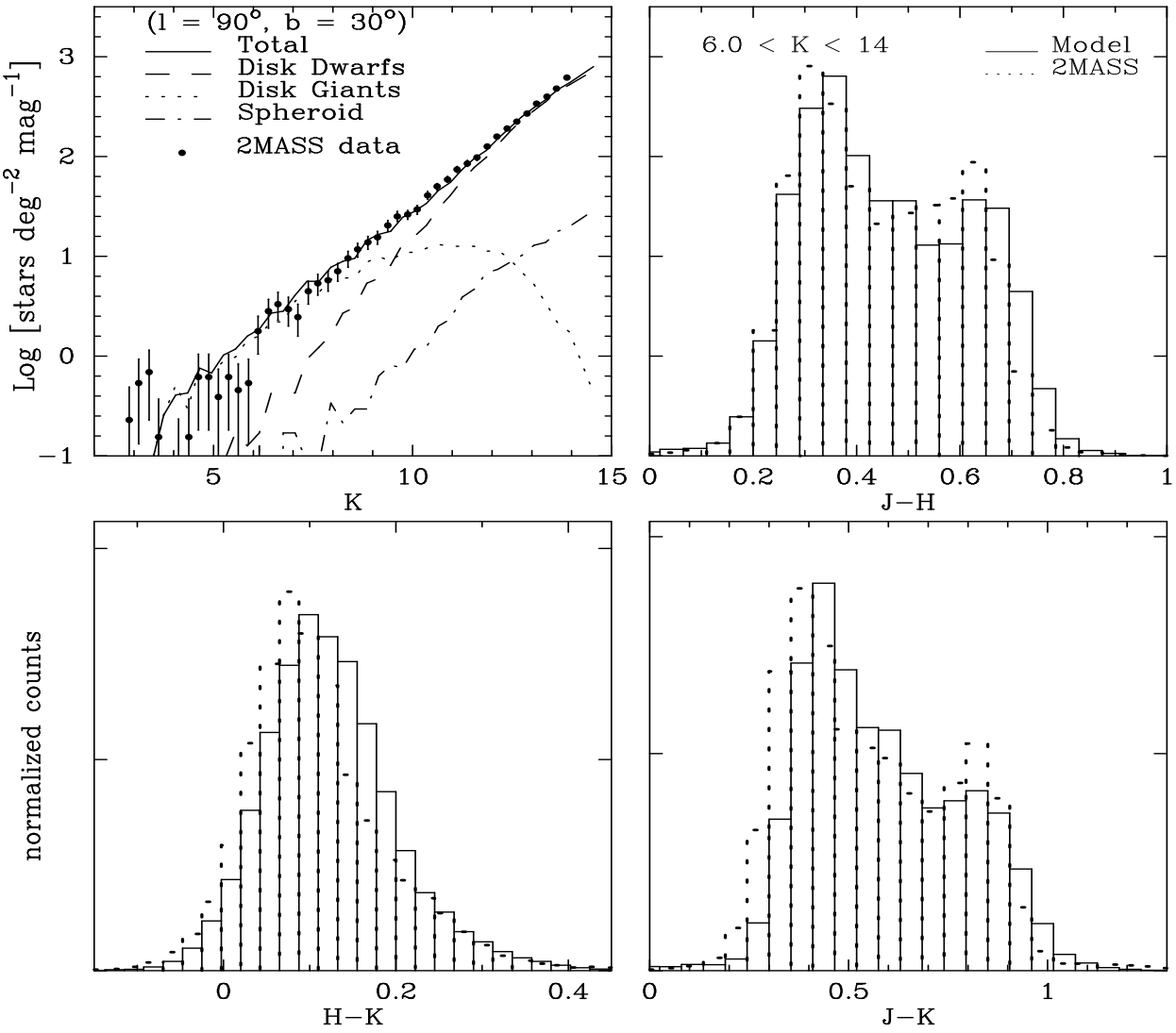

Fig. 13.— Star counts and colors for $l = 90°$, $b = 30°$. A $5° \times 5°$ 2MASS field, centered on galactic position $l = 90°$ $b = +30°$, is depicted with K_s-band star counts and $J - H$, $H - K_s$ and $J - K_s$ colors. The color histograms are restricted to $6 < K_s < 14$ mag. Overlaid are the model predictions.

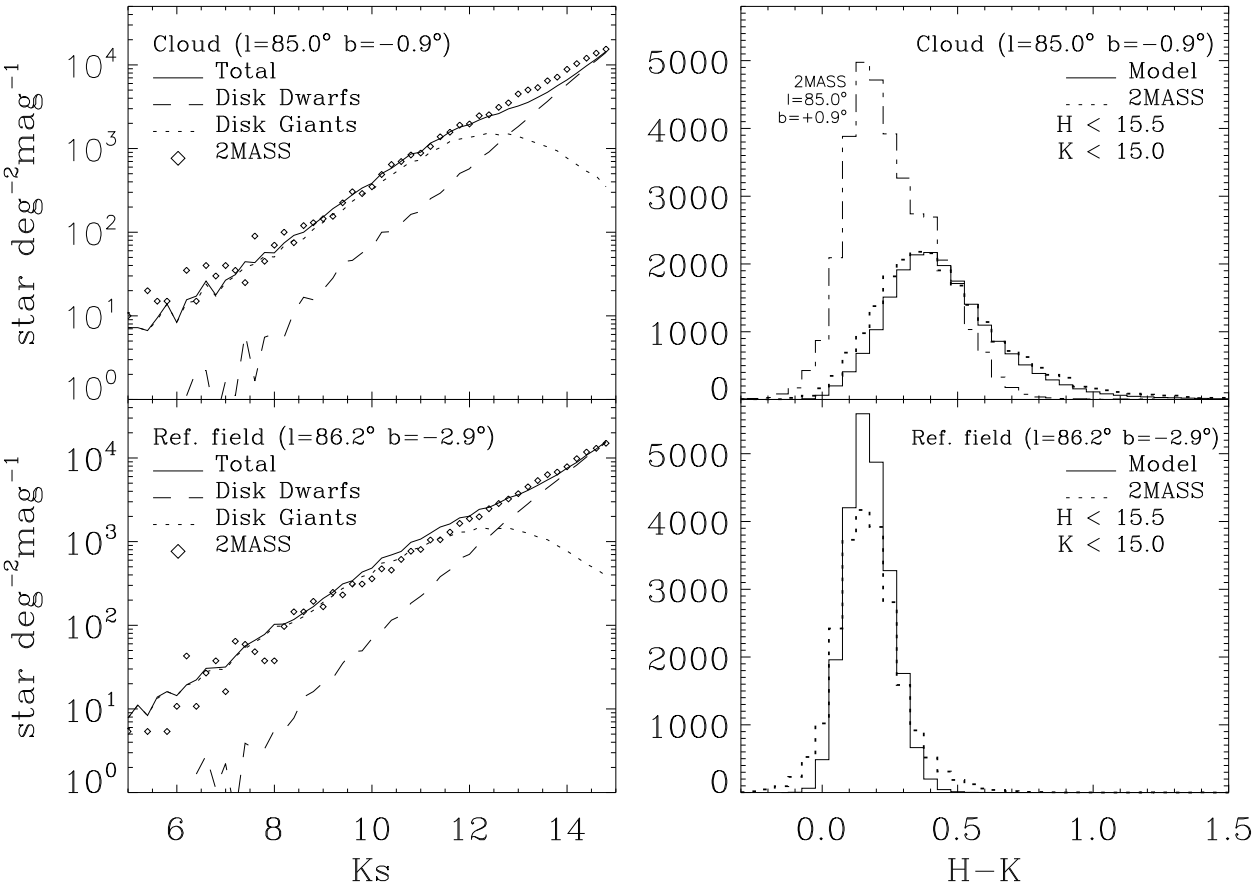

Fig. 14.— K_s-band star counts and $H - K_s$ colors for the NAN ($l = 85°$, $b = -0.9°$), upper panels, and the reference region ($l = 86.2°$, $b = -2.9°$), lower panels. The 2MASS measurements are depicted with diamond symbols. Overlaid (connected lines) are the model predictions. For comparison, the upper right panel includes the predicted $H - K_s$ colors for stars located along the line-of-sight that is directly opposite the NAN in the galactic plane ($l = 85°$, $b = +0.9°$; see also Table 2). NAN model includes extinction map.